Solid-State Synthesis of Monazite-type Compounds Containing Tetravalent Elements

Damien Bregiroux, Olivier Terra, Fabienne Audubert, Nicolas Dacheux, Virginie Serin, Renaud Podor, Didier Bernache-Assollant

Solid state synthesis of monazite-type compounds containing tetravalent elements

Damien Bregiroux[a,b], Olivier Terra[c], Fabienne Audubert[a], Nicolas Dacheux[c], Virgine Serin[d], Renaud Podor[e] and Didier Bernache-Assollant[f]*

[a], Commissariat à l'Énergie Atomique, DEN/DEC/SPUA/LTEC, Cadarache, 13108 Saint Paul Lez Durance, France

[b], Laboratoire Science des Procédés Céramiques et de Traitements de Surface, UMR-CNRS n°6638, 123 avenue Albert Thomas, 87060 Limoges, France

[c], Institut de Physique Nucléaire d'Orsay, Groupe de Radiochimie, Université Paris-Sud-11, 91406 Orsay, France

[d], Centre d'Elaboration de Matériaux et d'Etudes Structurales, Groupe Nanomatériaux, 29 rue Jeanne Marvig, BP 94347, 31055 Toulouse, France

[e], Laboratoire de Chimie du Solide Minéral, UMR-CNRS 7555, Université Henri Poincaré Nancy 1, BP 239, 54506 Vandoeuvre lès Nancy, France

[f], École Nationale Supérieure des Mines, CIS, 158 cours Fauriel, 42023 Saint Etienne, France

damien.bregiroux@ccr.jussieu.fr

* Corresponding author.

Present address: Université Pierre et Marie Curie - Paris 6, CNRS UMR 7574, Chimie de la Matière Condensée de Paris, 4, place Jussieu, Paris F-75005, France. Tel.: +33 144274770, Fax: +33 144272548

1. Introduction

In the framework of the French research law related to the specific conditioning of long life radionuclides in dedicated ceramics, phosphate matrices were extensively studied.[15] On the basis of several properties of interest such as weight loading,[6] sintering capability,[7,8] resistance to aqueous alteration[811] or to radiation damage,[12,16] monazites ($M^{III}PO_4$), brabantites ($M^{II}_{0.5}M^{IV}_{0.5}PO_4$) and associated monazite/brabantite solid solutions ($M^{III}_{1-2x}M^{II}_{x}M^{IV}_{x}PO_4$) were selected to perform advanced kinds of experiments through, as instance, the French Research Group NOMADE (CNRS/CEA/AREVA/EDF/French universities) in the field of the so called "Technical Feasability".[17] The synthesis of monazites, especially pointing out the preparation[1,18,], the process[2124] or the optimization of specific properties required[9,16] was already described. On the basis of their redox properties, the actinides considered for the development of such matrices, could be mainly trivalent (Pu, Am, Cm) or tetravalent (Th, U, Np, Pu) which strengthens the interest of designing matrices which could accept both tri- and tetravalent elements in their structure, *e.g.* $M^{III}_{1-2x}M^{II}_{x}M^{IV}_{x}PO_4$.[5,7]

From a geochemical point of view, monazite ($LnPO_4$ with Ln: La–Tb) is the most abundant lanthanide phosphate observed in natural samples.[25] Such minerals appear as the major thorium source on earth, especially in several ores which contain up to 14.3 wt.% and 15.6 wt.% in ThO_2 and UO_2, respectively.[26,27] Some other observations revealed the presence of samples containing up to 50 wt.% of thorium and consequently no indication of the presence of lanthanides in the minerals.[25,28,29] The incorporation of both tetravalent elements in the monazite structure was usually explained by the two following coupled substitutions:

$$2\ Ln^{3+} \Leftrightarrow (Th,U)^{4+} + Ca^{2+} \quad (1)$$

$$Ln^{3+} + PO_4^{3-} \Leftrightarrow (Th,U)^{4+} + SiO_4^{4-} \quad (2)$$

Some analyses carried out on natural samples revealed that the mechanism described by (eq 1) is widely predominant.[3032] It leads to a complete and ideal solid solution $M^{III}_{1-2x}M^{II}_{x}M^{IV}_{x}PO_4$, between pure monazite and pure brabantite ($M^{II}_{0.5}M^{IV}_{0.5}PO_4$).[33] Van Emden *et al.* also noted that in several samples containing cerium, the (Ca+Si) content was higher than (Th+U)[32] leading to the conclusion that

tetravalent cerium was probably incorporated in the monazite structure through both coupled substitutions. However, no analysis was carried out to validate this hypothesis. In the field of the second coupled substitution (eq 2), one of the $ThSiO_4$ form is isostructural from $LaPO_4$ (monoclinic system, S.G.: $P2_1/n$) which is not the case for $USiO_4$ (tetragonal system, S.G.: $I4_1/amd$). It is worth noting that $ThSiO_4$ could exist in both crystallographic forms;[34] the phase transition from tetragonal to monoclinic occurring at about 1200°C. Moreover, $USiO_4$ is unstable at temperatures higher than 500°C in air (1 atm.) and decomposes into UO_2 and SiO_2.[35;36]

The preparation of synthetic actinide bearing monazites was driven either by wet or dry chemistry methods. Among the methods based on wet chemistry processes, a large part involved the precipitation of initial crystallized precursors (*e.g.* rhabdophanes of formula $LnPO_4 \cdot ½H_2O$)[37] then an heating treatment above 700°C.

For trivalent actinides, these methods allowed the preparation of $AnPO_4$ (with An = U, Pu, Am-Bk). The incorporation of trivalent uranium, which appears rather curious from a redox point of view, was obtained in anoxic conditions and in presence of formic acid from a mixture of Na_3PO_4 and trivalent uranium solution.[38] The preparation of $PuPO_4$ was reported from $PuPO_4 \cdot ½H_2O$ precipitated between 75°C and 90°C from a mixture of trivalent plutonium and phosphoric acid in presence of concentrated sulphuric acid or from a mixture of plutonium trichloride and $(NH_4)_2HPO_4$.[39,40] After heating above 950°C, this blue well crystallized precursor was fully transformed into Pu-monazite.[40,41] More recently, the preparation of $La_{1-x}Am_xPO_4$ with large amounts of ^{241}Am was reported by Aloy *et al.*[42] from associated precipitated rhabdophanes. The same way was finally applied to prepare Am-monazite samples from Am-rhabdophane[43,44] at the gram scale and $CmPO_4$,[45,46] $BkPO_4$, $CfPO_4$ and $EsPO_4$ at the microgram scale.[46] The main conclusion is that, excepted for U-monazite which preparation remains doubtful due to the low stability of trivalent oxidation state of uranium, An-monazite samples can be obtained easily from plutonium to einsteinium by using wet chemistry methods.

On the contrary, some other actinides (Th, Pa, Np) can not be incorporated in their trivalent oxidation state in the monazite structure that requires their incorporation by the way of coupled substitution, as

described in (eq 1) and (eq 2). Moreover, brabantites and monazite/brabantite solid solutions are rather difficult to obtain through wet chemistry methods. In this field, Podor *et al.* synthesized several single crystals of $La_{1-2x}Ca_xAn_xPO_4$ solid solutions (with An(IV) = Th, U) by putting mixtures of $La(OH)_3$, $Ca(OH)_2$ or CaO and $An(OH)_4$ or AnO_2 with concentrated phosphoric acid in hydrothermal conditions near to geological conditions (t = 24 hours, T = 780°C, P = 200 MPa, Ni/NiO buffer to control the dioxygen fugacity and to avoid the oxidation of uranium (IV) into uranyl).[47,48] By this way, polyphase systems composed by $Ca_{0.5}U_{0.5}PO_4$ and $U_2(PO_4)(P_3O_{10})$[49] were always prepared, leading to the same conclusions than that given by Muto *et al.*[50]

According to literature, single crystals of monazite and monazite/brabantite solid solutions were usually prepared by the flux method from a mixture of rare-earth oxide and lead diphosphate at 1300°C.[51] The crystals of monazite (or monazite/brabantite), formed during the cooling step (975°C ≤ T ≤ 1300°C) were finally isolated by preferential dissolution of PbP_2O_7 in hot concentrated nitric acid. By the way, several authors reported the formation of samples doped with uranium (up to 10 wt.%), neptunium (3.0 wt.%), plutonium (6.0 wt.%), americium (up to 0.5 wt.%) or curium (0.1 wt.%).[6,52,53] While the formation of Am– or Cm–doped monazite samples is not surprising taking into account the stabilization of the trivalent oxidation state of these actinides, the incorporation of the two tetravalent actinides (U, Np) in monazite samples could not be explained by the formation of vacancies for the weight loadings considered but probably involves the formation of $Ln_{1-2x}Pb_xAn_xPO_4$ solid solutions as an explanation of such weight loadings with tetravalent actinides.[54] For Pu–doped samples, the stabilization of both oxidation states could be also evoked[39,40,55] even though the probability of the presence of Pu(III) appears to be more important on the basis of the reduction of Pu(IV) into Pu(III), as already discussed in literature.[56,57]

Consequently, the incorporation of high weight loadings of tetravalent actinides in the monazite structure requires one of the two coupled substitutions discussed in (eq 1) and (eq 2). This incorporation, which appears difficult to reach by wet chemistry methods, seems to occur only considering dry chemistry methods. Indeed, samples of $Ca_{0.5}An_{0.5}PO_4$ (An = Th, U or Np) were

prepared as single phase after heating a mixture of AnO_2, $CaCO_3$ and $(NH_4)_2HPO_4$ at high temperature under inert conditions.[58,59] Tabuteau et *al.* reported the formation of $Ca_{0.5}Np_{0.35}Pu_{0.15}PO_4$ through the simultaneous incorporation of tetravalent neptunium and plutonium.[59] According to some recent experiments, samples of $Pu^{III}_{0.4}Pu^{IV}_{0.3}Ca_{0.3}PO_4$ monazite/brabantite solid solution were also obtained at high temperature.[16] On the contrary, the application of the same procedure to the preparation of $Ca_{0.5}Pu_{0.5}PO_4$ remained unsuccessful, probably due to the reduction of Pu(IV) into Pu(III) during the heating treatment, leading to the formation of $PuPO_4$.[59] The same conclusion was given on the basis of several attempts to stabilize tetravalent cerium as $Ca_{0.5}Ce_{0.5}PO_4$. Heindl *et al.* used the high temperature solid state route to synthesize $M^{II}_{0.5}Ce^{IV}_{0.5}PO_4$ (with M^{II} = Ca, Ba and Sr).[60] All the resulting powders were green colored. Moreover, the XRD lines exhibited a shift towards the small 2θ angles compared to the diagram of $CePO_4$ which is not in agreement with the fact the ½(Ce^{IV}+Ca^{II}) couple is smaller than Ce^{III}. More recently, Pepin *et al.* performed the same experiment but observed neither green color, nor shift in the XRD lines. They also noted the presence of a secondary phase, $Ca_2P_2O_7$.[61] The relationship between the Ca content and the powder color of $(Ce,Ca)PO_4$ was recently used by Imanaka *et al.* and Sivakumar *et al.* for the elaboration of green pigments.[62;63] Nevertheless, the authors did not determine the valence state of cerium in these powdered samples.

On the basis of such results, Podor et *al.* described the limit of incorporation of tetravalent element in brabantite samples, $M^{II}_{0.5}M^{IV}_{0.5}PO_4$, *versus* the ionic radius of divalent cation, $\overline{^{IX}r(M^{II})}$, tetravalent cation, $\overline{^{IX}r(M^{IV})}$ and the average cationic radius $\overline{^{IX}r(M^{IV+II})}$ in the nine-fold coordination through the two following relationships:[47;48]

$$1.107\ \text{Å} \leq \overline{^{IX}r(M^{IV+II})} \leq 1.216\ \text{Å} \quad (3)$$

$$1.082 \leq \overline{^{IX}r(M^{II})} \Big/ \overline{^{IX}r(M^{IV})} \leq 1.238 \quad (4)$$

which becomes:

$$1.107\ \text{Å} \leq \overline{^{IX}r(M^{III+IV+II})} \leq 1.216\ \text{Å} \quad (5)$$

$$1 \leq \overline{^{IX}r(M^{III+II})} \Big/ \overline{^{IX}r(M^{III+IV})} \leq 1.238 \quad (6)$$

with $\overline{^{IX}r(M^{III+IV+II})} = (1-2x)\ ^{IX}r(M^{III}) + x\ ^{IX}r(M^{II}) + x\ ^{IX}r(M^{IV})$ (7)

and

$$\overline{^{IX}r(M^{III+II})} \Big/ \overline{^{IX}r(M^{III+IV})} = [(1-2x)\ ^{IX}r(M^{III}) + x\ ^{IX}r(M^{II})] \Big/ [(1-2x)\ ^{IX}r(M^{III}) + x\ ^{IX}r(M^{IV})] \quad (8)$$

when discussing about the simultaneous substitution of trivalent lanthanide by divalent and tetravalent cations in monazite/brabantite solid solutions, $M^{III}_{1-2x}M^{II}_{x}M^{IV}_{x}PO_4$.

Both $\overline{^{IX}r(M^{IV+II})}$ and $\overline{^{IX}r(M^{II})} \Big/ \overline{^{IX}r(M^{IV})}$ values were determined from (eq 3) and (eq 4), on the one hand, and from the ionic radii of actinides determined according to Shannon[64] with the assumption that the evolution of the actinide ionic size follows a linear function of the atomic number as well as in the eightfold coordination,[16] on the other hand. These values reach 1.105 Å and 1.14, 1.10 Å and 1.16 and 1.09 Å and 1.17 for $Ca_{0.5}Np_{0.5}PO_4$, $Ca_{0.5}Ce_{0.5}PO_4$ and $Ca_{0.5}Pu_{0.5}PO_4$, respectively. Based on these results, the formation of $Ca_{0.5}Pu_{0.5}PO_4$ and $Ca_{0.5}Ce_{0.5}PO_4$ brabantites would be difficult since the $\overline{^{IX}r(M^{IV+II})}$ value does not satisfy the inequality given in (eq 3) while that of $Ca_{0.5}Np_{0.5}PO_4$ and $Ca_{0.5}Np_{0.35}Pu_{0.15}PO_4$ remains possible, as described in literature. In the same way, the maximum incorporation of tetravalent actinide/element in $M^{III}_{1-2x}M^{II}_{x}M^{IV}_{x}PO_4$ was evaluated for M^{III} = La and M^{II} = Ca. The results are reported in Table 1. One can note that the coupled substitution 2 $Ln^{III} \Leftrightarrow M^{IV} + M^{II}$ would not be complete for cerium (x_{max} = 0.47) or plutonium (x_{max} = 0.45).

Table 1. Ionic radii of some tetravalent actinides in the ninefold coordination and their maximum incorporation in $LaPO_4$ ($La_{1-2x}M^{IV}_{x}Ca_{x}PO_4$)

M^{IV}	Ce	Th	U	Np	Pu
$\overline{^{IX}r_{M(IV)}}$	1.02 Å	1.09 Å	1.05 Å	1.03 Å	1.01 Å
$x_{max.}$	0.47	0.50	0.50	0.49	0.45

The aim of this paper is thus to investigate (reexamine) the incorporation of three tetravalent elements (Th, U, Ce) in the brabantite structure through high temperature solid state route. In this work, thorium is considered on the basis of its stabilized tetravalent oxidation state which excludes other redox

reactions. On the contrary, tetravalent uranium that can be oxidized and cerium (used as a plutonium surrogate) that can be reduced have been considered in a second part of the work. A particular aspect of this study consists in the description of the schematic scheme of incorporation of these three tetravalent elements (Th, U, Ce) in the brabantite structure, as a preliminary work dedicated to the formation of monazite/brabantite solid solutions including tetravalent thorium and/or uranium.

2. Experimental section

All the samples were prepared by firing initial mixtures containing MO_2, $Ca(HPO_4)\cdot 2H_2O$ (or CaO for cerium compounds) and $NH_4H_2PO_4$.[1,17] In order to increase the reactivity of the initial mixtures, the starting materials were ground for few minutes by mechanical grinding in zirconia bowls before being fired under inert atmosphere (M = U and Th) or in air (M = Ce) in alumina boats with heating and cooling rates of $10°C.min^{-1}$. In the field of the improvement of the final homogeneity of the samples, the optimization of the grinding conditions was already described for several phosphate ceramics doped with thorium and/or uranium such as thorium phosphate-diphosphate solid solutions, britholites, monazites and monazite/brabantite solid solutions.[7]

The thermal behaviour of the mixtures was followed by differential thermal analysis (DTA) and thermogravimetry (TG) using a Setaram TG 92–16 apparatus in platinum crucibles. All the XRD analyses were performed on powdered samples at room temperature using a Bruker D8 Advance X-ray diffractometer (Cu K_α = 0.15418 nm). The unit cell parameters were refined using U–Fit or PowderCell software.[65,66]

The Electron Probe MicroAnalyses (EPMA) experiments were carried out using Cameca SX 50 and SX 100 apparatus (operating with an acceleration voltage of 15 kV and a current intensity of 10 nA). The calibration standards used were mainly $LaPO_4$ and $CePO_4$ monazites (K_α emission of phosphorus and L_α emission of cerium, respectively), wollastonite Ca_2SiO_4 (K_α emission of calcium), ThO_2 (M_α emission of thorium) and $UO_{2.12}$ (M_β emission of uranium). It is worth noting that some interferences were detected during the EPMA analyses in the samples containing simultaneously large amounts of

calcium and uranium, leading to the systematic over-estimation of the calcium content, as already discussed for $Ca_9Nd_{0.5}U_{0.5}(PO_4)_{4.5}(SiO_4)_{1.5}F_2$ (U-britholites) samples.[3]

μ-Raman spectra were recorded with a microspectrometer LABRAM (Dilor – Jobin Yvon) using an argon laser operating at 514.5 nm with a power in the range 1-10 mW. The sample position was checked thanks to an Olympus microscope.

Transmission electron microscopy (TEM) and Electron Energy Loss Spectroscopy (EELS) analyses were performed in the SACTEM–Toulouse, using a Tecnai F20 (FEI) equipped with an objective lens aberration corrector (CEOS) and imaging filter (Gatan Tridiem).

3. Results and discussion

3.1. Preparation of $Ca_{0.5}Th_{0.5}PO_4$

The synthesis of $Ca_{0.5}Th_{0.5}PO_4$ was followed, from a starting mixture of $Ca(HPO_4)\cdot 2H_2O$, ThO_2 and $NH_4H_2PO_4$, *versus* the heating temperature ($400 \leq T \leq 1400$°C) using DTA/TG experiments (Figure 1).

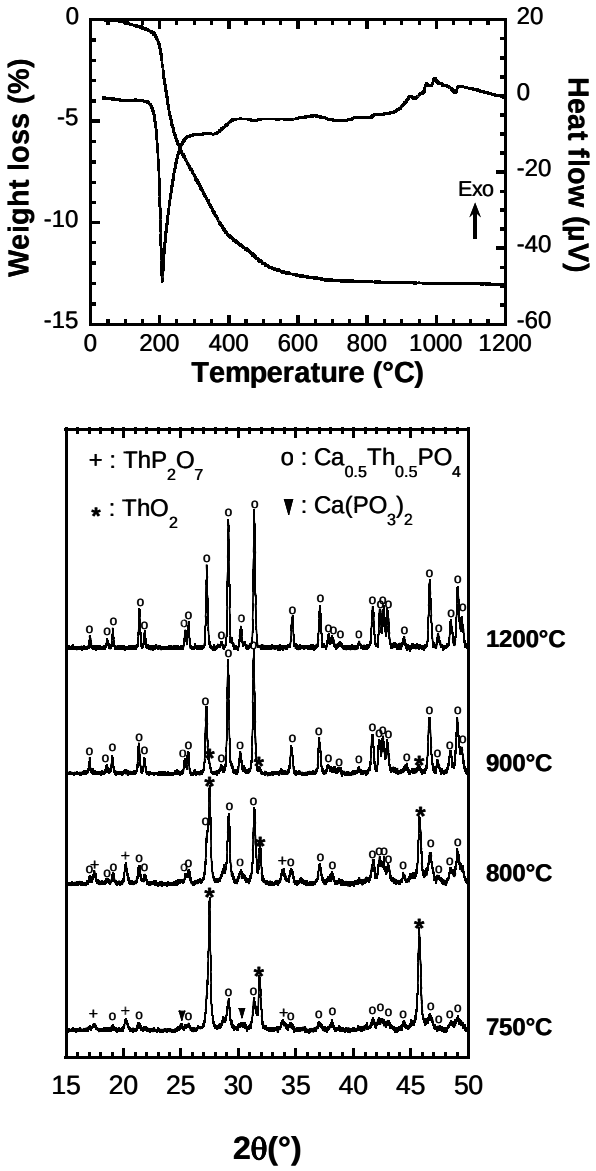

Figure 1. Thermal analysis under argon and X-ray diffraction analysis of a ThO_2-$Ca(HPO_4)\cdot 2H_2O$-$NH_4H_2PO_4$ mixture.

The total weight loss observed on the TG curves (i.e. ≈ 13%) occurs in several steps below 600°C. It was associated with the dehydration of $Ca(HPO_4)\cdot 2H_2O$ and to the decomposition of $NH_4H_2PO_4$. Between 180°C and 400°C, the total weight loss (≈ 10.8%) was associated with three endothermic effects located at 208°C, 360°C and 474°C, assigned to the release of water, to the condensation of hydrogenphosphate groups into polytrioxophosphate entities and finally to the quantitative release of NH_3.[67] No additional weight loss is observed above 600°C while several exothermic effects are

observed at 777°C, 827°C, 925°C, 970°C and 994°C, due to reactions occurring between several intermediates as discussed thereafter. Some of these peaks were globally associated to the formation then decomposition of thorium diphosphate (α–ThP_2O_7), calcium polytrioxophosphate ($Ca(PO_3)_2$) and to the formation of Th–brabantite (*i.e.* $Ca_{0.5}Th_{0.5}PO_4$).

The chemical reactions occurring during the formation of Th–brabantite was also followed *versus* the heating temperature through XRD on samples heated at several temperatures ranging from 400 to 1400°C (Figure 1). Between 400 and 700°C, the XRD patterns always reveal the presence of ThO_2 [JCPDS File # 42–1462] while the XRD lines of $Ca(HPO_4)\cdot 2H_2O$ and $NH_4H_2PO_4$ progressively disappear for the benefit of that of $Ca(PO_3)_2$ [JCPDS File # 9–363] formed as an intermediate product. Above 750°C, all the XRD lines of Th–brabantite are observed [JCPDS File # 31–311] as a consequence of the reaction between $Ca(PO_3)_2$ and ThO_2. Simultaneously, the XRD lines of α–ThP_2O_7 are also observed [JCPDS File # 16–230]. This intermediate progressively disappears above 900°C. Between 800 and 900°C, the system appears thus polyphase and consists on a mixture of $Ca_{0.5}Th_{0.5}PO_4$, $Ca(PO_3)_2$, ThO_2 and α–ThP_2O_7 between which several chemical reactions occur leading to the numerous effects observed during the DTA experiments. The thermal effects observed between 700 and 1000°C are surely the consequence of several solid-solid reactions between all these compounds. Nevertheless, these effects can not be easily discriminated which contributes to some difficulties in their specific assignment, as already mentioned.

Above 1000°C, the XRD patterns correspond to pure and single phase Th–brabantite[68] which chemical composition is consistent with that expected (Table 2).

Table 2. EPMA results of $Ca_{0.5}M_{0.5}PO_4$ synthesized at 1200h for 6 hours in inert atmosphere

	M = Th		**M = U**	
	Obs.	Calc.	Obs.	Calc.
wt.% (O)	25.2 ± 0.2	27.7	28.3 ± 0.4	27.3

wt.% (P)	14.0 ± 0.2	13.4	13.6 ± 0.2	13.24
wt.% (Ca)	9.0 ± 0.1	8.7	9.3 ± 0.1*	8.6
wt.% (An)	51.8 ± 0.6	50.2	51.5 ± 0.8	50.9
M/Ca	1.00 ± 0.02	1	0.94 ± 0.02*	1
P/(Ca+M)	1.01 ± 0.01	1	0.982 ± 0.008	1

The spectroscopic characterization of $Ca_{0.5}Th_{0.5}PO_4$ through μ-Raman experiments confirms that all the vibration bands observed correspond to δ_S(P–O) (400 – 450 cm^{-1}), δ_{AS}(P–O) (530 – 650 cm^{-1}), ν_S(P–O) (≈ 980 cm^{-1}) and ν_{AS}(P–O) (1050 – 1150 cm^{-1}) associated to PO_4 entities as reported in Figure 2.

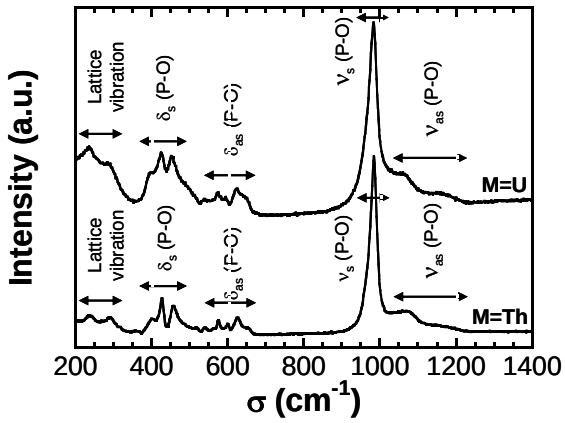

Figure 2. μ-Raman spectra of $Ca_{0.5}M_{0.5}PO_4$.

All the data recorded appear in good agreement with that reported in literature.[69] Moreover, no vibration band associated of the P–O–P bridge characteristic of diphosphate entities or of polytrioxophosphate groups is observed (especially in the range of 700 – 800 cm^{-1})[70] that confirms the complete reaction between intermediates such as α-ThP_2O_7 and $Ca(PO_3)_2$.

Finally, the crystallinity of the Th–brabantite phase was followed through the determination of the average FWHM of the main XRD lines, corresponding to the $\bar{1}11$, $20\bar{1}$, 120, 012, $20\bar{2}$ and 112 reflections (Figure 3), and of the refined unit cell parameters (Table 3).

* Interferences revealed during analyses, between uranium and calcium, leading to an overestimation of calcium

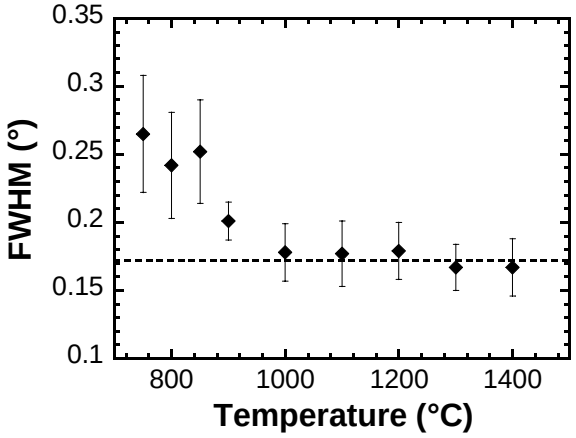

Figure 3. Average FWHM of the main XRD lines (i.e. $\bar{1}11$, $20\bar{1}$, 120, 012, $20\bar{2}$ and 112) of $Ca_{0.5}Th_{0.5}PO_4$, *versus* synthesis temperature.

Table 3. Unit cell parameters of $Ca_{0.5}M_{0.5}PO_4$ *versus* synthesis temperature under Ar atmosphere

	T (°C)	a (nm)	b (nm)	c (nm)	β (°)	V×10^3 (nm^3)	F_{20}
M=Th	Podor *et al.*[48]	0.6714	0.6921	0.6424	103.68	290.0	-
	750	0.6728(4)	0.6918(3)	0.6432(3)	103.89(4)	290.6(4)	<10
	800	0.6724(2)	0.6912(3)	0.6419(5)	103.94(4)	289.6(5)	13(0.0017;85)
	900	0.67156(7)	0.69153(5)	0.64190(6)	103.797(9)	289.5(7)	73(0.0051;54)
	1000	0.67118(4)	0.69155(5)	0.64170(4)	103.753(6)	289.3(5)	90(0.0054;41)
	1100	0.67120(4)	0.69152(5)	0.64168(5)	103.737(7)	289.3(5)	89(0.0057;39)
	1200	0.67123(4)	0.69169(5)	0.64163(5)	103.738(6)	289.4(5)	115(0.0051;34)
	1300	0.67139(4)	0.69185(5)	0.64201(4)	103.737(6)	289.7(5)	103(0.0050;39)
	1400	0.67137(4)	0.69181(5)	0.64187(4)	103.732(6)	289.6(5)	96(0.0055;38)
M=U	Montel *et al.*[68]	0.6673	0.6852	0.6364	104.07	282.3	-
	900	0.6675(2)	0.6853(2)	0.6372(2)	104.10(3)	283(2)	20(0.015;66)
	1000	0.66728(5)	0.68590(5)	0.63733(6)	104.037(8)	283.0(2)	81(0.0039;63)
	1100	0.66729(3)	0.68607(4)	0.63755(5)	104.036(6)	283.2(5)	92(0.0036;61)
	1200	0.66724(4)	0.68601(5)	0.63766(6)	104.028(8)	283.2(6)	125(0.0039;41)
	1300	0.66718(4)	0.68596(5)	0.63765(6)	104.025(7)	283.1(6)	70(0.0047;61)
	1400	0.66706(3)	0.68607(4)	0.63782(5)	104.020(7)	283.2(5)	85(0.0041;57)

From these data, it is clear that the cristallinity of Th–brabantite samples is significantly improved when increasing the heating temperature from 750 to 1200°C, the optimized conditions of preparation being obtained between 1200 and 1300°C. At these temperatures, the unit cell parameters obtained (a =

6.7123(4) Å, *b* = 6.9169(5) Å, *c* = 6.4163(5) Å and β = 103.738(6)°) appear in good agreement with the data reported in the literature for Th–brabantite samples prepared through other chemical processes which confirms the full incorporation of thorium in the monazite structure through the coupled substitution examined.[47,71] Finally, at 1400°C, the refinement of the unit cell parameters seems to indicate the beginning of the thermal decomposition of $Ca_{0.5}Th_{0.5}PO_4$, which was especially observed when increasing the heating time at this temperature. For higher heating temperatures, some small amounts of thorium dioxide were also detected at the surface of the samples (especially when working on Th–brabantite pellets), as a consequence of the local decomposition of Th–brabantite into calcium oxide, thorium dioxide and volatile phosphorous oxide (P_4O_{10}), according to:

$$Ca_{0.5}Th_{0.5}PO_4 \xrightarrow{T \geq 1400°C} \tfrac{1}{2}CaO + \tfrac{1}{2}ThO_2 + \tfrac{1}{4}P_4O_{10}\uparrow \qquad (9)$$

3.2. Preparation of $Ca_{0.5}U_{0.5}PO_4$

From the results reported in the previous section, the full incorporation of thorium in the monazite structure appears possible when heating between 1200 and 1300°C. However, as already discussed, thorium is expected to be only tetravalent in these operating conditions of synthesis. For this reason, the incorporation of uranium which presents several stabilized oxidation states (mainly (IV) and (VI) in phosphoric medium) was also examined. In this aim, mixtures of UO_2, $Ca(HPO_4)\cdot 2H_2O$ and $NH_4H_2PO_4$ were ground mechanically then fired at several heating temperatures ranging from 400 to 1400°C.

The first indication of the progression of the solid–solid reaction was deduced from some changes in the colour of the samples which turned from black/grey (due to the presence of UO_2 in the mixture) to green (characteristic of the presence of tetravalent uranium in phosphoric compounds)[72,73] when heating above 900°C. Such an observation was correlated to the study of the variation of the XRD diagrams *versus* the heating temperature (Figure 4) which indicates that the incorporation of uranium in the monazite structure follows the same chemical scheme than that reported for thorium. Indeed, after the full dehydration of $Ca(HPO_4)\cdot 2H_2O$ then the decomposition of $NH_4H_2PO_4$ between 100°C and 600°C, the XRD pattern highlights the presence of $Ca(PO_3)_2$ and α–UP_2O_7 [JCPDS File # 16–263], as

intermediates above 700°C. All the XRD lines of U–brabantite ($Ca_{0.5}U_{0.5}PO_4$) are observed when heating above 900°C, correlatively to the decrease of the XRD lines of UO_2 [JCPDS File # 41–1422]. At this temperature, the $Ca_{0.5}U_{0.5}PO_4$ phase [JCPDS File # 12–279] coexists with UO_2 and α–UP_2O_7 which fully disappear at 900°C and 1000°C, respectively.

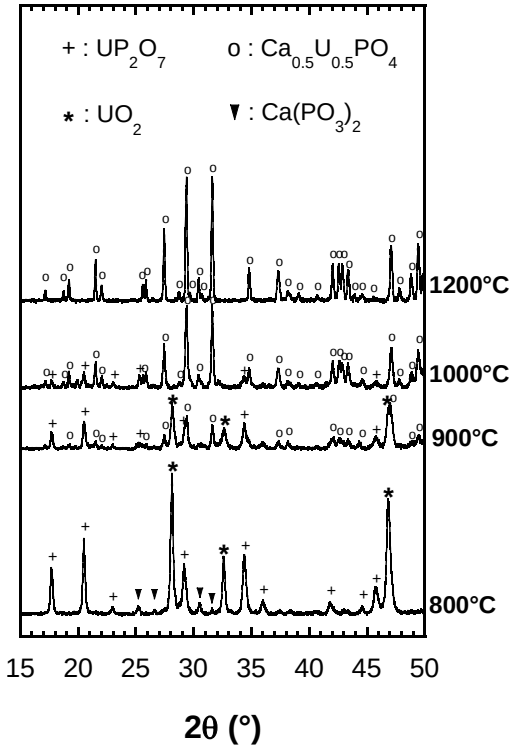

Figure 4. X-ray diffraction analysis of a UO_2-$Ca(HPO_4)\cdot 2H_2O$-$NH_4H_2PO_4$ mixture.

Pure and single phase samples of U–brabantite are thus obtained when heating above 1100°C. At this temperature, the elementary composition determined from EPMA appears in good agreement with that expected (Table 2) while the unit cell parameters determined (Table 3) seems to confirm the incorporation of tetravalent uranium in the monazite structure.[48]

The comparison of the μ-Raman spectra of $Ca_{0.5}Th_{0.5}PO_4$ and $Ca_{0.5}U_{0.5}PO_4$ does not reveal any significant differences (Figure 2). The positions of the vibration bands are very close, particularly the strong one located around 980 cm^{-1} (which can be assigned to ν_S(P-O) in phosphate groups). As for Th–brabantite, it is worth noting that the vibrations usually associated to diphosphate or

polytrioxophosphate groups are not observed, as a confirmation of the complete reaction of the intermediates formed at lower temperatures (α–UP_2O_7 or $Ca(PO_3)_2$). Moreover, the absence of intense and narrow vibration band in the domain 850–870 cm^{-1}, characteristic of the ν_1 symmetric stretching mode of uranyl units (UO_2^{2+})[74,76] confirms the stabilization of tetravalent uranium during all the synthesis process which was suggested by the colour of all the final samples prepared, as already discussed. These results appear in contradiction with that reported by Mc Carthy *et al.*[77] who observed the oxidation of uranium (IV) during the heating treatment and also with the data associated to the synthesis of U–britholites[3] which revealed the formation of $CaUO_4$ then CaU_2O_{5+y} through a complex redox uranium cycle.

As it was observed for Th–brabantite, the cristallinity of U–brabantite is significantly improved when increasing the heating temperature from 900 to 1200°C (decrease of the average FWHM and improvement in the unit cell parameters refinement). Above 1300°C, the beginning of the decomposition of U–brabantite is observed, leading to the formation of uranium dioxide (which can be evidenced by the change in colour form green to grey/black). This decomposition is particularly observed at the surface of U–brabantite pellets which are finally recovered by this thin black/grey uranium oxide layer when extending the heating time. As already discussed for Th–brabantite, the associated reaction of decomposition can thus be written:

$$Ca_{0.5}U_{0.5}PO_4 \xrightarrow{T \geq 1300°C} \tfrac{1}{2}\ CaO + \tfrac{1}{2}\ UO_2 + \tfrac{1}{4}\ P_4O_{10}\uparrow \qquad (10)$$

On the basis of the results obtained when studying the formation of Th–brabantite and U–brabantite from mixtures of MO_2 (M = Th, U), $Ca(HPO_4)\cdot 2H_2O$ and $NH_4H_2PO_4$, a simplified chemical mechanism was proposed (Figure 5).

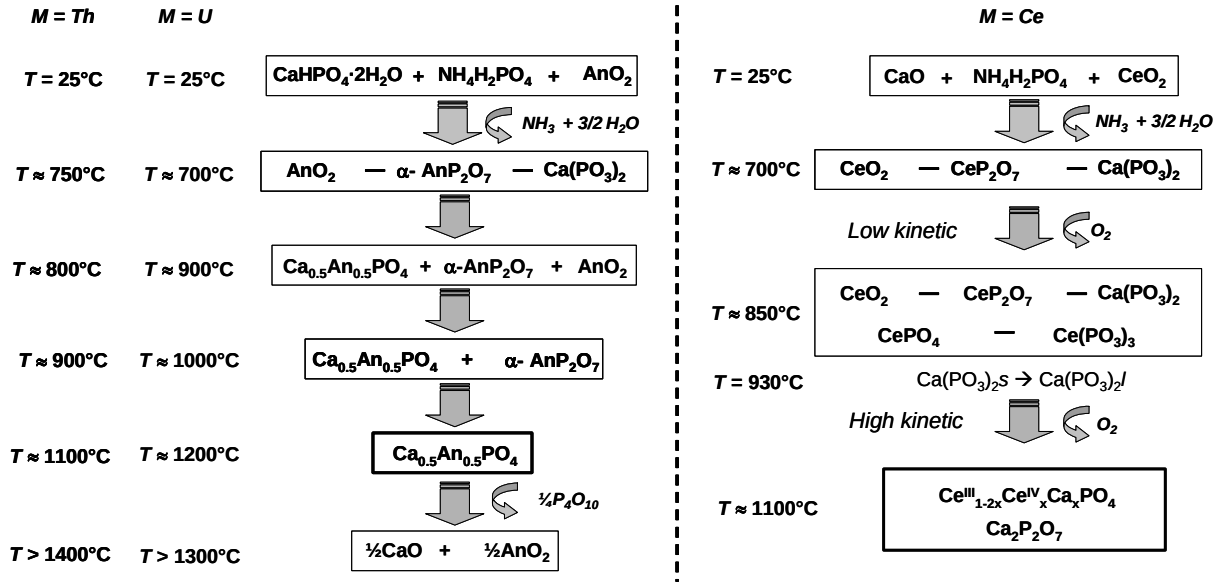

Figure 5. Thermal behavior of the starting mixture under argon atmosphere (for Th and U) or in air (for Ce).

3.3. Synthesis of $Ca_{0.5}Ce_{0.5}PO_4$

As uranium, plutonium could exist with two stabilized oxidation states (III and IV) in the phosphate environment. However, the trivalent oxidation state appears as the most favorable plutonium oxidation state in the monazite structure. Nevertheless, it is questionable if Pu(IV) could exist in such a structure when calcium is simultaneously incorporated. Because of the radiotoxicity of plutonium, experiments were first developed with cerium as a surrogate, since cerium presents similar properties with plutonium, both in terms of ionic size and redox properties. To this aim, the thermal behavior of a CeO_2–CaO–$2NH_4H_2PO_4$ mixture was investigated.

The physical and chemical phenomena occurring during the calcination of the starting mixture were followed by thermal analysis and by XRD for $Ca_{0.5}Ce_{0.5}PO_4$ (Figure 6).

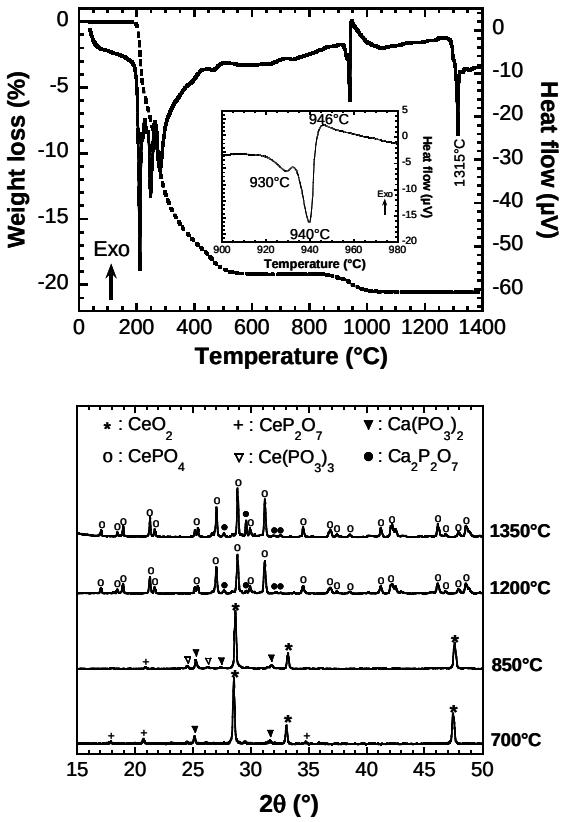

Figure 6. Thermal analysis under air and X-ray diffraction of a CeO_2-CaO-$2NH_4H_2PO_4$ mixture.

From room temperature to 800°C, several thermal effects and an important weight loss were observed, all assigned to the thermal decomposition of $NH_4H_2PO_4$ into NH_3 and H_2O, as previously observed for thorium (see section 3.1.). The observed weight loss (19.23%) is very close to the expected value (19.22%). Beyond 800°C, 4 thermal effects (930°C, 940°C, 946°C and 1315°C) and an additional weight loss (1.44% between 800°C and 1050°C) could be observed. With the TG derivative curve, not plotted on this graph, the latter can be assigned as the second endothermic effect occurring at 940°C. The analysis of the emitted gas by mass spectrometry revealed that this weight loss is due to a dioxygen emission. As already described for thorium and uranium, the XRD patterns revealed the presence of monazite and of calcium diphosphate $Ca_2P_2O_7$ [JCPDS File # 73-0440], as previously described by Pepin *et al.*[61] Moreover, three other phosphates could be observed as transient compounds: CeP_2O_7 [JCPDS File # 30–0164] and $Ca(PO_3)_2$ at 700°C and 850°C, and $Ce(PO_3)_3$ [JCPDS File # 33–0336] at 850°C. Melting points of $Ca(PO_3)_2$ and $Ca_2P_2O_7$, measured by thermal analysis, was found to be located

at 985°C and 1318°C, respectively. From these results, the qualitative mechanism of reaction can be proposed (Figure 5). The reactions can be sorted into two categories:

(a) Solid state reactions (T < 930°C)

– From 40°C to 840°C, the phosphate precursor melts and decomposes with emission of NH_3 and H_2O before reacting with CaO and CeO_2 to form $Ca(PO_3)_2$ and CeP_2O_7:

$$2NH_4H_2PO_4 + CaO + CeO_2 \rightarrow Ca(PO_3)_2 + CeP_2O_7 + 2NH_3\uparrow + 3H_2O\uparrow \quad (11)$$

– From 840°C to 930°C, a slight weight loss is observed on the TG curve (Figure 6). According to literature, this results of the slow decomposition of α–CeP_2O_7:[1,78,79]

$$2CeP_2O_7 \rightarrow Ce(PO_3)_3 + CePO_4 + \tfrac{1}{2}O_2\uparrow \quad (12)$$

The oxygen emission appears as the consequence of the reduction of the Ce(IV) into Ce(III).

(b) Liquid state reactions (930°C < T < 1050°C)

– At 930°C, $Ca(PO_3)_2$ melts (DTA effect at 930°C) and dissociates into Ca^{2+} and PO_3^-:[80]

$$Ca(PO_3)_{2(s)} \rightarrow [Ca^{2+} + 2\ PO_3^-]_\ell \quad (13)$$

– In such an ionic liquid, the Ce–O chemical bond of CeO_2 is probably broken[80] Consequently, the liquid phase consists of 4 ions, *i.e.* $Ca^{2+} + 2PO_3^- + Ce^{4+} + O^{2-}$. Immediately, the kinetic of the reduction of Ce^{4+} strongly increases (DTA effect at 940°C). Consecutively, a slow precipitation of two phases occurs (wide DTA effect at 946°C):

$$[Ca^{2+} + Ce^{3+} + 2PO_3^- + 3/2O^{2-}]_\ell \rightarrow CePO_{4(s)} + \tfrac{1}{2}Ca_2P_2O_{7(s)} \quad (14)$$

The DTA effect observed at 1315°C can thus be assigned to the melting of $Ca_2P_2O_7$. In conclusion, the chemical reaction occurring during the calcination of a CeO_2–CaO– $2NH_4H_2PO_4$ is, with the assumption that it is a total reaction:

$$CeO_2 + CaO + 2NH_4H_2PO_4 \rightarrow CePO_4 + \tfrac{1}{2}Ca_2P_2O_7 + 2NH_3\uparrow + 3H_2O\uparrow + \tfrac{1}{4}O_2\uparrow \quad (15)$$

However, several experiments indicate that the reaction reported in (eq 15) is not complete and that the powder contains both trivalent and tetravalent cerium. The resulting powder exhibits a green color,

as observed by Heindl *et al.*,[60] whereas $CePO_4$ is usually white colored. Moreover, the unit cell parameters are smaller (a = 6.711 Å, b = 7.036 Å and c = 6.384 Å) than that reported for pure $CePO_4$ (a = 6.800 Å, b = 7.024 Å and c = 6.474 Å),[1] which appears in agreement with the partial incorporation of Ce(IV) in the monazite structure, since ½(Ce^{IV}+Ca^{II}) is smaller than Ce^{III} (1.10 Å and 1.196 Å, respectively).[64] The presence of Ce^{IV} in the monazite structure was highlighted without any ambiguity by EELS (Figure 7).

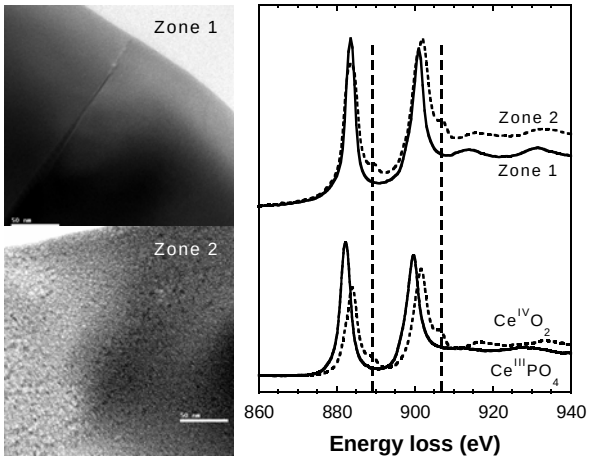

Figure 7. TEM observation and cerium EELS spectra of $M_{4,5}$-edge fine structure of CeO_2-CaO-$2NH_4H_2PO_4$ mixture fired at 1400°C.

Two different types of zones were observed by TEM. The first one appears with a uniform contrast and an amorphous structure (*Zone 1* on Figure 7), while in the second one, cristallized nanostructures were observed (*Zone 2* on Figure 7). The analysis of the fine structure of the cerium $M_{4,5}$–edge doublet leads to several remarks:

- the spectra of *Zone 1* is characteristic of trivalent cerium;
- the shift of the doublet toward the high energies, the extra shoulders observed in *Zone 2* spectra and the inversion of the intensity ratio between the two peaks prove the presence of Ce(IV) in this zone, in agreement with experiments performed on Ce^{III} and Ce^{IV} references samples and with litterature.[81,82] Moreover, calcium is only detected in the *Zone 2*, which is consistent with the presence of Ce^{IV} in this zone.

3.4. Incorporation of Ce^{IV} in $(La,Ce)^{III}PO_4$ solid solution

The previous results highlight that only a small amount of tetravalent cerium could be incorporated in the monazite structure. Two hypotheses could explain this incomplete incorporation: tetravalent cerium is unstable in monazite because of redox properties, or the (Ce^{IV},Ca^{II}) couple is too small to incorporate the monazite structure. In that case, the incorporation should be linked to the global cationic size. Thus, the Ce^{IV}/Ce^{III} ratio should be higher in a $LaPO_4$ matrix than in a $CePO_4$ one. Consequently, the incorporation of the (Ce^{IV},Ca^{II}) couple is investigated in the $LaPO_4 – CePO_4$ solid solution:

$$\tfrac{1}{2}(1–2x)La_2O_3 + xCeO_2 + xCaO + NH_4H_2PO_4 \rightarrow La_{1-2x}Ce^{III}_{x-y}Ce^{IV}_{y}Ca_y(PO_4)_{1-x+y} + \tfrac{1}{2}(x–y)Ca_2P_2O_7 + NH_3\uparrow + \tfrac{1}{2}H_2O\uparrow + \tfrac{1}{4}(1–2x)O_2\uparrow \quad (16)$$

The measurement of Ce^{IV}/Ce^{III} ratio was obtained by using two methods:

(a) EPMA experiments: in the monazite phase, the amount of tetravalent cerium was determined by measuring both Ca and Ce contents, noted (Ca) and (Ce), respectively, with the assumption that Ca^{2+} acts as the only charge compensation mechanism. The Ce^{IV}/Ce^{III} mole ratio is thus given by the following relationship:

$$\frac{Ce^{IV}}{Ce^{III}} = \frac{(Ca)}{(Ce) - (Ca)} \quad (17)$$

This method is all the more accurate than (Ce) and (Ca) is high (i.e. for high x values). For the samples examined in this work, EPMA was not suitable for $x < 0.2$.

(b) XRD analysis: this method was based on the refinement of the unit cell parameters of the monazite phase from which it is possible to deduce the average cationic radius $\overline{^{IX}r(M^{III+II+IV})}$ considering, as instance, the following relation:[1]

$$\overline{^{IX}r(M^{III+II+IV})} = \frac{a - 0.4718}{1.7420} \quad (18)$$

with:

$$\overline{^{IX}r(M^{III+II+IV})} = \frac{(1-2x)\times {}^{IX}r_{La} + y \times {}^{IX}r_{Ce^{IV}} + y \times {}^{IX}r_{Ca^{II}} + (x-y)\times {}^{IX}r_{Ce^{III}}}{1 - x + y} \quad (19)$$

which allows the determination of *y* according to:

$$y = \frac{(1-2x)\times {}^{IX}r_{La} + x \times {}^{IX}r_{Ce^{III}} - (1-x)\times \overline{{}^{IX}r(M^{III+II+IV})}}{\overline{{}^{IX}r(M^{III+II+IV})} - {}^{IX}r_{Ce^{IV}} - {}^{IX}r_{Ca^{II}} + {}^{IX}r_{Ce^{III}}} \quad (20)$$

Based on the unit cell parameters determined, this method exhibits a constant accuracy, whatever the *x* value considered.

All the results reveal the presence of tetravalent cerium in monazite/brabantite samples (Table 4, Figure 8). Nevertheless, the incorporation rate appears weak, *i.e.* $Ce^{IV}/(\Sigma \text{ cations}) < 10\%$, which is lower from the expected value (47%), exclusively obtained on the basis of sterical criteria (eqs 3-4 and Table 1).

Table 4. Determination of Ce^{IV}/Ce^{III} in monazite by XRD and EPMA

	XRD			EPMA			
x	$\overline{{}^{IX}r}$ **(Å)**	***y***	**Ce^{IV}/Ce^{III}**	**(Ca)**	**(Ce)**	***y***	**Ce^{IV}/Ce^{III}**
0.04	1.214 ± 0.001	0.007 ± 0.001	0.20 ± 0.01	0.018 ± 0.004	0.035 ± 0.008	0.02 ± 0.01	1.0 ± 0.7
0.06	–	–	–	0.018 ± 0.002	0.04 ± 0.02	0.02 ± 0.01	0.6 ± 0.4
0.08	1.212 ± 0.001	0.010 ± 0.001	0.15 ± 0.01	0.018 ± 0.002	0.086 ± 0.008	0.017 ± 0.004	0.28 ± 0.1
0.10	1.211 ± 0.001	0.013 ± 0.001	0.15 ± 0.01	0.019 ± 0.002	0.091 ± 0.008	0.021 ± 0.005	0.27 ± 0.09
0.15	1.210 ± 0.001	0.011 ± 0.001	0.08 ± 0.01	–	–	–	–
0.20	1.206 ± 0.001	0.020 ± 0.001	0.11 ± 0.01	0.027 ± 0.002	0.25 ± 0.04	0.022 ± 0.005	0.12 ± 0.04
0.25	1.205 ± 0.001	0.017 ± 0.001	0.07 ± 0.01	–	–	–	–
0.30	1.203 ± 0.001	0.015 ± 0.001	0.05 ± 0.01	0.040 ± 0.007	0.416 ± 0.02	0.029 ± 0.006	0.12 ± 0.04
0.35	1.198 ± 0.001	0.023 ± 0.001	0.07 ± 0.01	–	–	–	–
0.40	1.198 ± 0.001	0.015 ± 0.001	0.04 ± 0.01	0.040 ± 0.005	0.81 ± 0.07	0.020 ± 0.004	0.06 ± 0.02
0.50	1.188 ± 0.001	0.022 ± 0.001	0.05 ± 0.01	0.050 ± 0.007	0.95 ± 0.01	0.026 ± 0.004	0.06 ± 0.01

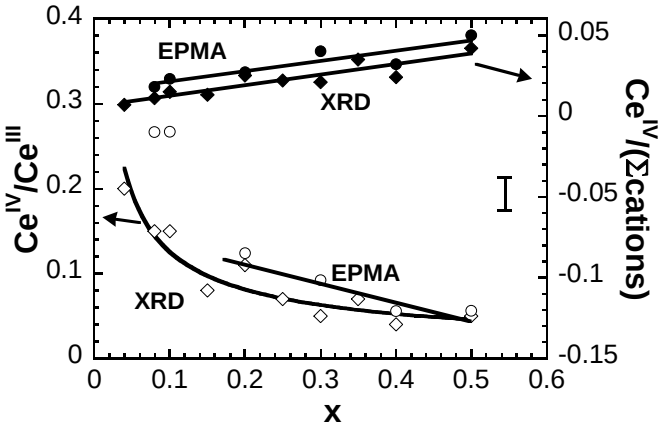

Figure 8. Incorporation of Ce^{IV} in $(La,Ce)^{III}PO_4$ solid solution

Moreover, $Ce^{IV}/(\Sigma cations)$ does not appears as a function of x . This highlights that the incorporation of the tetravalent form of an element in the monazite crystal structure is governed by the redox potential of the M^{4+}/M^{3+} couple with regard to O_2/O^{2-}. Unfortunately, the redox potentials of the M^{4+}/M^{3+} couples remain unknown in the conditions of synthesis considered. Nevertheless, it is possible to discuss on the basis of the values at 25°C – 1 atm.[83] In these conditions, the redox potential of Pu^{4+}/Pu^{3+} and Ce^{4+}/Ce^{3+} are close to O_2/O^{2-} (1.006V, 1.72V and 1.12V, respectively), which is in accordance with the existence of monazite containing both tri- and tetravalent cerium (this work) and plutonium.[16] Since the coexistence of the M^{IV} and M^{III} in monazite is all the more important as the redox potential of the M^{4+}/M^{3+} couple is close the one of O_2/O^{2-}, this can also easily explain why Pu^{IV} is incorporated in $LaPO_4$ at an higher level than Ce^{IV} ($\frac{M^{IV}}{M^{IV}+M^{III}}$ = 0.5 for plutonium and 0.1 for cerium, respectively).

4. Conclusion

Acknowledgment. The authors are grateful to Johan Ravaux and Alain Kolher from LCSM (Université Henri Poincaré Nancy-I, France) for performing EPMA and SEM experiments and to Thérèse Lhomme from CREGU (Université Henri Poincaré Nancy-I, France) for her extensive help

during the characterization of the samples by the μ-Raman technique. This work was financially and scientifically supported by the French Research Group NOMADE (GdR 2023, CNRS/CEA/COGEMA) and by a CEA-CFR research grant.

TOC GRAPHIC

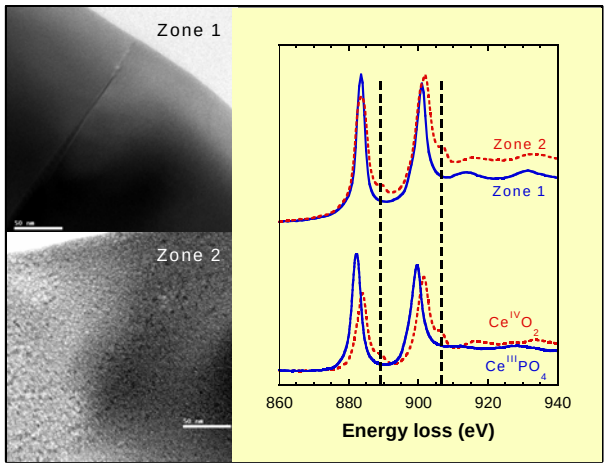

(1) Bregiroux, D.; Audubert, F.; Charpentier, T.; Sakellariou, D.; Bernache-Assollant, D. *Solid State Sci.* **2007**, 9, 432-439.

(2) Terra O., Audubert F., Dacheux N. Guy C. and Podor R., *J. Nucl. Mater.*, 354 (2006) 49.

(3) Terra O., Audubert F., Dacheux N. Guy C. and Podor R., *J. Nucl. Mater.*, 366 (2007) 70.

(4) Clavier N., Dacheux N., Podor R., *Inorg. Chem.*, 45 (2006) 220.

(5) Dacheux N., Clavier N., Robisson A.C., Terra O., Audubert F., Lartigue J.E., Guy C., *C.R. Acad. Sc. Paris*, 7 (2004) 1141.

(6) Boatner L.A., Beall G.W., Abraham M.M., Finch C.B., Hurray P.G., Rappaz M., in *: "Scientific Basis for Nuclear Waste Management"*, Eds C.J.M. Northrup Jr., New York, Vol. 2, 289, **1980**.

(7) Terra O., Dacheux O., Audubert F. and Podor R., *J. Nucl. Mater.*, 352 (2006) 224.

(8) Terra O., Clavier N., Dacheux N., Podor R., *New J. Chem.*, 27 (2003) 957.

(9) Poitrasson F., Oelkers E.H., Schott J. and Montel J.-M., *Geochim. Cosmchim. Acta*, 68 (2004) 2207.

(10) Oelkers E.H. and Poitrasson F., *Chem. Geol.*, 191 (2002) 73.

(11) Cetiner Z.S., Wood S.A. and Gammons C.H., *Chem. Geol.*, 217 (2005) 147.

(12) Ewing R.C. and Haaker R.F., *Nuclear and Chemical Waste Management*, 1 (1980) 51.

(13) Karioris F.G., Appaji Gowda K. and Cartz L., *Rad. Eff. Lett.*, 58(1-2) (1981) 1

(14) Meldrum A., Boatner L.A., Weber W.J. and Ewing R.C., *Geochim. Cosmochim. Acta*, 62 (1998) 2509.

(15) Burakov B.E., Yagovkina M.A., Garbuzov V.M., Kitsay, A.A. and Zirlin V.A., *Mater. Res. Soc. Symp. Proc.*, 824 (2004) 219.

(16) Bregiroux D., Belin R., Valenza P., Audubert F., Bernache-Assollant D., *J. Nucl. Mater.* 366 (2007) 52.

(17) Deschanels X. *Evaluation de la Faisabilité Technique des Nouvelles Matrices de Conditionnement des Radionucléides à Vie Longue*; Technical Report DTCD/2004/5; Commissariat à l'Energie Atomique (CEA)-Département d'Etudes du Traitement et du Conditionnement des Déchets (DTCD): Paris, 2004.

(18) Su M.Z., Zhou J. and Shao K.-S., *J. Alloys Compd*, 207-208 (1994) 406.

(19) Onoda H., Nariai H., Maki H. and Motooka I., *Mater. Chem. Phys.*, 73 (2002) 19.

(20) Hikichi Y., *Mineral. J.*, 15 (1991) 268.

(21) Hikichi Y., Nomura T., Tanimura Y. and Suzuki S., *J. Am. Ceram. Soc.*, 73 (1990) 3594.

(22) Hikichi Y. and Ota T., *Phosph. Res. Bull.*, 6 (1996) 175.

(23) Bregiroux D., Lucas S., Champion E., Audubert F. and Bernache-Assollant D., *J. Eur. Ceram. Soc.*, 26 (2005) 279.

(24) Bregiroux D., Audubert F. and Bernache-Assollant D., *Adv. Sci. Tech.*, 45 (2006) 633.

(25) Förster H.J., *Am. Mineral.*, 83 (1998) 259.

(26) Gramaccioli C.M. and Segalstad T.M., *Am. Mineral.*, 63 (197(8) 757.

(27) Boatner L.A., in : « *Review in mineralogy and chemistry* », 48 (2002) 87.

(28) Montel J.M., Kornprobst J., Vielzeuf D., *J. Metamorph. Geol.*, 3 (2000) 335.

(29) Förster H.J., Harlov D.E., *Mineralogical Magazine*, 63 (1999) 587.

(30) Kucha H., *Mineral. Mag.*, 43 (1980) 1031.

(31) Rose R., *N. Jb. Miner. Mh.*, H(6) (1980) 247.

(32) Van Emden B., Thornber M.R., Graham J. and Lincoln F.J., *Can. Mineral.*, 35 (1997) 95.

(33) Rose D., *N. Jb. Miner. Mh.*, H6 (1980) 247.

(34) Mazeina L., Ushakov S.V., Navrotsky A. and Boatner L.A., *Geochim. Cosmochim. Acta*, 69 (2005) 4675.

(35) Hoekstra H.R. and Fuchs L.H., *Science*, 123 (1956) 105.

(36) Fuchs L.H. and Hoekstra H.R., *Am. Miner.*, 44 (1959) 1057.

(37) Lucas S., Champion E., Bregiroux D., Bernache-Assolant D., Audubert F., *J. Solid St. Chem.*, 177 (2004) 1302.

(38) Drozdzynski J., *Inorg. Chim. Acta*, 32 (1979) L83.

(39) C.E. Bamberger, R.G. Haire, H.E. Hellwege, G.M. Begun, *J. Less Common Metals*, 97 (1984) 349.

(40) C.W. Bjorklund, *J. Am. Chem. Soc.*, 79 (1957) 6347.

(41) Cleveland J.M., in : "*The chemistry of plutonium*", Ed. Gordon & Breach Science Publishers, New-York, 1970.

(42) Aloy A.S., Kovarskaya E.N., Koltsova T.I., Samoylov S.E., in : "*Radioactive Waste Management and Environmental Remediation"*, ASME, **2001**.

(43) Keller C., Walter K.H., *J. Inorg. Nucl. Chem.*, 27 (1965) 1253.

(44) Rai D., Felmy A.R., Fulton R.W., *Radiochim. Acta*, 56 (1992) 7.

(45) Weigel F., Hauy H., *Radiochim. Acta*, 4 (1965) 327.

(46) Hobart D.E., Begun G.M., Haire R.G., Hellwege H.E., *J. Raman Spectro.*, 14 (1983) 59.

(47) Podor R., Cuney M., *Am. Miner.*, 82 (1997) 765.

(48) Podor R., Cuney M., Nguyen-Trung C., *Am. Miner.*, 80 (1995) 1261.

(49) Podor R., François M., Dacheux N., *J. Solid State Chem.*, 172 (2003) 66.

(50) Muto T., Merowitz R., Pommer A.M., Murano T., *J. Am. Mineral.*, 44 (1959) 633.

(51) Feigelson R.S., *J. Am. Ceram. Soc.*, 47, (1964) 257.

(52) Kelly K.L., Beall G.W., Young J.P., Boatner L.A., in : *"Scientific Basis for Nuclear Waste Management"*, Eds J.G. Moore, New York, Vol. 3, 189, **1981**.

(53) Mullica D.F., Sappenfield E.L., Wilson G.A., *Lanthanide and Actinide Res.*, 3 (1989) 51.

(54) Montel J.M., Devidal J.L., *EUG XI, Symposium PCM6*, Cambridge Publication, 680, **2001**.

(55) Seaborg G.T., in : *"Plutonium Chemistry"*, Eds. W.T. Carnall & G.R. Choppin, ACS, Washington, **1983**.

(56) Bamberger C.E., Begun G.M., Brynestad J., Land J.F., *Radiochim. Acta*, 31 (1982) 57.

(57) Dacheux N., Podor R., Brandel V., Genet M., *J. Nucl. Mater.*, 252 (1998) 179.

(58) Pepin G.J., Vance E.R., McCarthy G.J., *Mat. Res. Bull.*, 16 (1981) 627.

(59) Tabuteau A., Pagès M., Livet J., Musikas C., *J. Mat. Sc. Let.*, 7 (1988) 1315.

(60) Heindl R., Flemke E. and Loriers J., *Conf. Dig.-Inst. Phys.*, (1971) 222.

(61) Pepin J.G., Vance E.R., McCarthy G.J., *Mater. Res. Bull.*, 16 (1981) 627.

(62) Imanaka N., Masui T. and Itaya M., *Chem. Lett.*, 32(4) (2003) 400.

(63) Sivakumar V. and Varadaraju U.V., *Bull. Mater. Sc.*, 28(3) (2005) 299.

(64) Shannon R.D., *Acta Crystallogr.*, A32 (1976) 751.

[65] Evain M., « *U-Fit program* », Institut des Matériaux de Nantes, France, 1992.

[66] Kraus W. and Nolze G., *J. Appl. Cryst.* 29 (1996) 301.

[67] Abdel-Kader A., Ammar A.A. and Saleh S.I., *Thermochim. Acta*, 176 (1997) 293.

[68] Montel J.M., Devidal J.L. and Avignant D., *Chem. Geol.*, 191 (2002) 89.

[69] Podor R., Eur. *J. Mineral.*, 7 (1995) 1353.

[70] Dacheux N., Brandel V., Genet M., *New J. Chem.*, 19 (1995) 15.

(71) Montel, J.M.; Glorieux, B.; Seydoux-Guillaume, A.M.; Wirth, R. J. *Phys. Chem. Solids* **2006**, *67*, 2489-2500.

[72] Bénard P., Louër D., Dacheux N., Brandel V., Genet M., *Chem. Mater.*, 6 (1994) 1049.

[73] Dacheux N., Brandel V., Genet M., *New J. Chem.*, 19 (1995) 1029.

[74] Frost R.L., Weier M.L., Martens W. and Cejka J., *Vibrational Spectroscopy*, 41 (2006) 205.

[75] Frost R.L., Weier M.L., *Spectrochim. Acta*, A(60) (2004) 2399.

[76] Thomas A.C., Dacheux N., Le Coustumer P., Brandel V. and Genet M., *J. Nucl. Mater.*, 295 (2001) 249.

[77] McCarthy G.J., White W.B. and Pfoertsch D.E., *Mat. Res. Bull.*, 13 (1978) 1239.

[78] Botto I.L. and Baran E.J., *Z. Anorg. Allg. Chem.*, 430 (1977) 283.

[79] Brandel V., Dacheux N., J. Solid St. Chem., 177 (2004) 4743.

[80] Pascal P., *Nouveau Traité de Chimie Minérale*, X (1956) Masson, Paris.

[81] Garvie L.A.J. and Busek P.R., *J. Phys. Chem. Solids*, 60 (1999) 1943.

[82] Colettan M., *J. Mater. Sci. Lett.*, 21 (2002) 1797.

[83] Lide D.R., *Handbook of Chemistry and Physics*, 73rd edition (1993) CRC Press.